Proceedings World Geothermal Congress 2000
Kyushu - Tohoku, Japan, May 28 - June 10, 2000

CORROSION INDUCED BY STEAM CONDENSATES IN UPPER MAHIAO PIPELINE, LEYTE, PHILIPPINES

Ruperto R. Villa, Jr. and Noel D. Salonga

PNOC Energy Development Corporation, Ft. Bonifacio, Makati City, Philippines

Keywords: condensate induced corrosion, steam condensate disposal, polarization, stress corrosion cracking

ABSTRACT

Polarization experiments made using different types of metal immersed in Upper Mahiao condensate line were conducted to elucidate the processes that control corrosion. Results showed that low carbon steel is incapable of forming a protective layer because of the continued breakdown of the protective film. Austenitic stainless steel showed a very wide passivation zone, suggesting that they will resist corrosion in this type of fluid.

Field experiments in Upper Mahiao steam condensate and condensate reinjection pipeline indicate unacceptable corrosion rates for carbons steels to be used in this environment. These results suggest poor passivation particularly in the presence of small amount of air. SEM, EPMA, XRD and XRF analyses were conducted on the corrosion samples to determine the actual chemical composition and the morphology of the corrosion products.

1.0 INTRODUCTION

In December 1997, the Geothermal Combined Cycle Power Plant was commissioned in the Upper Mahiao sector of the Tongonan Geothermal Field, Leyte, Philippines. The plant has a net capacity of 125 MW and has the world's largest network of air-cooled non-contact cooling towers (Forte, 1996). At full load, the power plant produces a total of 270 kg/s steam condensate obtained from the heat-exchange system. The condensate is saturated with dissolved CO_2 and H_2S gases that promoted acid attack on the condensate pipelines barely three months from the start of operation. To evaluate the problem of condensate pipeline corrosion, two field material tests were conducted at Upper Mahiao. The aim of these tests was to identify an economical material that could withstand the corrosive nature of the condensates. Although both tests showed that low carbon steel is not resistant to this type of fluid, the test did not clearly explain the corrosion mechanism in the pipeline.

Thus, polarization experiments were conducted at Kyushu University Material Science Laboratory to shed light on the corrosion mechanism involved. Moreover, an extensive analysis of the corrosion samples from the field tests in aerated condensate using Scanning Electron Microscope (SEM), Electron Probe Micrograph Analysis (EPMA), X-Ray Diffraction (XRD) and X-Ray Fluorescence (XRF) Analysis was conducted at the Kyudensangyo Industries Laboratory to identify the corrosion processes and corrosion product morphology.

2.0 POWER PLANT PROCESS FLOW AND CONDENSATE DISPOSAL

The power plant operation is based on a Geothermal Combined Cycle Unit (GCCU). The unit is a combination of a back pressure steam turbine generator (STG) operating at high pressure and at around 180~188 ^oC followed downstream by sets of Ormat Energy Converter (OEC) systems operating on an Organic Rankine Cycle (Forte, 1996). These OEC's basically consist of shell-and-tube heat exchanger which vaporize the organic binary fluid (n-pentane) to drive the attached low-pressure turbine. A simplified process flow of this power plant is presented in Figure 1. From the OEC heat exchangers, the fully condensed steam is separated from the Non-Condensable Gases (NCG) at a temperature between 50-60 ^oC. While the NCG is treated in the Abatement Plant prior to its dispersal to the atmosphere, all the condensates are piped downstream in a low carbon steel pipeline towards the spray tower (Fig. 2). The temperature drops further at the spray tower to meet the environmental guidelines prior to mixing with river water.

Although the Non-Condensable Gases (NCG) were separated from the condensate, it is still saturated with CO_2 and H_2S gases after separation from the OEC as shown by its typical chemistry listed in Table 1. These gases control the acidity and are considered as the primary factors that promote corrosion attack (Salonga et al., 1998). During the first three months of Upper Mahiao power plant operation (December 1996 to March 1997), problems were encountered at the condensate pipeline. The downstream spray tower nozzles were often clogged with black solid particles which were composed of FeS_2 and Fe_2O_3. Line maintenance required diverting the flow using a separate alvenius (galvanized) pipeline to facilitate declogging of the nozzles (Fig. 2). Three (3) months later in March 1997, a long crack (around 2 meters) was observed at the bottom part of the pipe causing severe leakage (Villa, 1997). Radiographic and ultrasonic testing revealed severe pipe thinning at the bottom of the pipe.

This event caused concern and material testing was done to identify an economic material suitable for long-term use (Salonga et al., 1997). Given the acidic nature of condensate, long term disposal was at risk because of reinjection pipeline and borehole corrosion.

3.0 SUMMARY OF FIELD MATERIAL TESTING

The material testing consisted of two parts. The first testing was conducted from July to September 1997 in hot steam condensate taken from the main steam lines utilizing aan aerated and non-aerated vessel at 50-100°C and the other was conducted from March to May 1998 at the condensate pipeline using similar set-up.

The first experiment indicated that stainless steels SUS 304 and SUS 316 are resistant to the condensate-induced corrosion. The other materials tested (low carbon steel and drill pipe) were not resistant, except, for the alvenius (galvanized) pipe material which showed some resistance in areas where the galvanized coatings were intact. The second experiment affirmed the conclusions of the first experiment. Moreover, it gave the following additional findings:

(1) the condensate is largely composed of dissolved CO_2 gas with significant amount of H_2S and NH_3 ;
(2) dissolved sulfur exists primarily as H_2S at lower oxidation potential (Eh) and as SO_4 at higher Eh. Native sulfur is only expected to form when there aeration;
(3) the fluids will favor the formation of free corrosion products of Fe^{++}, and thus, uniform corrosion will always occur (Figure 3). Pyrite is the most probable passive film that will form and hematite will form simultaneously or as a secondary product of pyrite at high Eh when air is present;
(4) less resistant coupons are affected by uniform and pitting corrosion (Salonga et al, 1998). Given the standard acceptable corrosion rate of 0.2 mm/yr., this suggests that alvenius (galvanized) pipe, low carbon steels and drill pipe corrosion rates >0.2 mm/yr. are not appropriate materials. Only SUS-304 and SUS-316 (rate <0.20 mm/yr.) are appropriate. Using this material will have no danger in chloride, sulfide or stress corrosion cracking since its operation is only limited to 60 ^oC.

4.0 ANALYSES OF PIPELINE CORROSION SAMPLES

The surface morphology of the low carbon steel pipeline corrosion samples from Test 2 (aerated condensate) appeared in the SEM as a rough formation dominated mainly by Fe and S components (Table 2). The EPMA and XRF results showed that Si (as SiO_2) and Ca are almost negligible. Moreover, the cross-sectional structure of these samples from the SEM showed a distinct layer of corrosion.

The lower portion showed a fine-grained layer while the upper portion showed a grainy (hexagonal and tetrahedral) layers which are soft and brittle. Based on XRD analysis, the upper layer is that of $FeSO_4.H_2O$ while the lower layer are that of FeS_2. These products confirm two possible reactions taking place inside the pipeline. The first reaction is the uniform corrosion brought by sulfide and iron reaction forming the pyrite layer. The second reaction of pyrite, steel and H_2S with water and atmospheric oxygen forming $FeSO_4.H_2O$, that worsens the corrosion problem. The atmospheric oxygen possibly encroached in the line during shutdowns. Hydrated ferrous sulfate is non-protective and oxygen will promote localized corrosion and the low carbon steel pipeline will never have a chance to form a protective layer to prevent the further advancement of corrosion.

5.0 CORROSION ASSESSMENT BY POLARIZATION STUDIES

Aqueous corrosion processes are usually electrochemical in nature. Corrosion mechanisms can be elucidated by electrochemical means through a study of the response of metal to controlled polarization (Romanov, 1969). Based on the processes involved in the Upper Mahiao operation, the corrosion mechanism can likely be explained by this method. When a current flows into a galvanic cell, for example, the anode becomes more cathodic in potential and the cathode becomes more anodic, the difference of potential becomes smaller. The extent of potential change caused by net current flow to or from an electrode of the galvanic cell is called polarization (Uhlig, 1985).

Measuring and recording the response of an electrode to polarization during a corrosion experiment can be used to study the following: (1) the kinetics of corrosion processes; (2) optimum protective current if cathodic or other protection is to be applied; (3) rates and limiting process (anodic or cathodic); (4) the influence of cathodic contacts on the corrosion of construction materials; and (5) effects and influence of inhibitors and contaminants.

In practice, polarization curves are often plotted to elucidate the influence of a number of factors on the corrosion rate one time. These factors usually influence certain stage of the cathodic and anodic processes. The degree to which any stage of the anodic or cathodic processes is inhibited or enhanced is characterized by rate of change of the potential as the current increased or decreased i.e. the slope of the polarization curves. Consequently, from the slopes of the curves it is possible to determine not only the type of the process being investigated but also which fundamental reactions governing these processes are influenced by a given factor.

Figure 4 gives a schematic presentation of the processes involved in an ideal polarization curve. The graph has four characteristic sections: (1) activation; (2) passivation; (3) oxygen evolution; and (4) hydrogen evolution. Activation is the cathodic depolarization at the corresponding corrosion current and potential which is due to the reduction of oxygen on the local microcathodes. On the other hand, the shape of passivation curve is determined by inhibition of the diffusion of oxygen to the microcathodes. At high potentials, oxygen is evolved at the surface of the polarized electrode and corrosion is rapid, typically by localized attack or pitting corrosion. The hydrogen evolution curve represents corrosion currents and potential at which the cathodic process dominates by evolution of hydrogen at the test electrode. The degree of the extent of corrosion can be estimated based on the amount of current density it absorbed at specific potential.

Polarization experiments were carried out using 4 alloys (see Table 3) exposed to Upper Mahiao disposal line condensate brought to the laboratory. The collected solutions contained some dissolved oxygen and but at low levels such that the concentration of SO4 would have remained low over the course of the test. Alternatively, exposure to air resulted in some dissolved oxygen being present. Table 4 gives the original chemistry of the test solution. The test solutions were heated to 60°C but were not further de-aerated. The test electrodes were initially held at potential of -1 V vs Ag/AgCl reference electrode and the potential was increased at a rate of 2.6 E-4 mV/s from the cathodic polarization region until about 1.5 to 1.8 mV anodic polarization was achieved. Ecor values achieved are typical for this experimental procedure with the carbon steel having a potential of -710 mV vs Ag/AgCl (-475 mV vs SHE), the austenitic stainless steels SUS-304 and 316 having potentials of -128 and -62 mV vs Ag/AgCl (+107 and +173 mV vs SHE) respectively and the martensitic SUS-410 stainless steel being between the carbon steel and the austenitic

stainless steels at –325 mV vs Ag/AgCl (-90 mV vs SHE), Table 5.

The anodic polarization curve of Figure 5 for carbon steel indicates active corrosion and no passive film formation. An interesting observation was the formation of brown deposits when carbon steel was immersed in the test solution indicating the presence of oxygen and a tendency for a hematite formation. These active/passive potentials are in accord with the potential-pH diagram of Figure 3 which shows carbon steel will freely corrode as the potential is swept from cathodic to anodic potentials. The metal is in a region of Fe+2 stability at pH 5.48 and the kinetics of formation of pyrite will be slow in this solution.

A small potential range of passivity is suggested for the SUS-410 (from –130 mV to +32 mV vs Ag/AgCl) and above this potential the alloy actively corrodes. Above this potential range the protective film is destroyed and pitting corrosion was observed to occur.

The SUS-304 and 316 show good passivity up to 600 mV vs Ag/AgCl. Normally, SUS-316 would be expected to show superior performance over SUS-316 whereas in this experiment they were very similar. This result is believed to be due to deterioration of the surface quality of SUS-316 specimen after a number of polarization experiments.

Corrosion rates can also be calculated from the polarization curves through graphical method by finding the intersect of the Tafel slope with the projected E_{cor}. The corresponding i_{cor} at this intersecting point (Fig. 4) can be used to determine the corrosion rates through the modified Faradays law equation (Pound et al., 1979):

$$CR = (I_{cor}*M)/zAF\rho \qquad \text{- equation (1)}$$

where CR is the corrosion rate (mm/yr), I_{cor} is the corrosion current (A), M is the molar mass of metal (g/mole), A is area of electrode (mm^2), z is number of electrons transferred per metal atom, F is the Faraday's constant and ρ is the density of metal (g/mm3). But i_{cor}, the current density, is equal to current applied per unit area of coupon. Therefore the above equation can be rewritten as:

$$CR = (i_{cor}*M)/zF\rho \qquad \text{- equation (2)}$$

Listed in Table 5, are the E_{cor}, i_{cor} and the CR of the metals tested. Based on this theoretical calculation of corrosion rates from its polarization curves in Figure 5, low carbon steel corrosion rate is 52.5 times higher than SUS-304 while the rate from SUS-410 is 1.9 times higher than SUS-304. Note that this experiment was conducted under static fluid flow laboratory conditions. In high velocity dynamic conditions, carbon steel rate will increase several times higher because of erosion effects. Given a 0.2 mm/yr. acceptance criteria for pipeline corrosion rate, low carbon steel is indeed unacceptable. Under conditions of fluid aeration the corrosion potential of the freely corroding alloys will increase naturally to a higher Eh and will approach the area marked UM in Figure 3. At a potential of 0 mV vs SHE or –235 mV vs Ag/AgCl the corrosion current for carbon steel in Figure 5 is about 2E-3 A/cm2 which corresponds to the corrosion rate (CR) of 210 mm/yr. Such heavy aeration is not expected to be encountered but the polarization result illustrates the potentially damaging influence of oxygen. Thus, a more resistant material is needed to handle this fluid i.e. SUS-304 or SUS-316.

The presence of air leads to the formation of corrosive sulfur species and the risk of chloride and sulfide induced Stress Corrosion Cracking (SCC) with the austenitic stainless steels SUS-304 and SUS-316. The levels of chloride present in the Upper Mahiao condensate reinjection line are low in comparison with those reported to give SCC of these alloys in mixed chloride/sulfide containing environments (Lichti et al, 1995). The resistance of SUS-316 is however far superior to SUS-304 in at-risk solutions and hence the selection of SUS-316 alloy would be preferred.

6.0 FUTURE CONDENSATE DISPOSAL

Condensates disposed directly into reinjection wells may result to damage to the low carbon steel wellbore casings. Alternative disposal options include mixing the condensates with the reinjection brine prior to disposal at a ratio not potentially hazardous to field operations and application of corrosion inhibitor or neutralizing agent.

Although the mixing of low temperature condensates (50-60 ^oC) with hot brine (160-180 ^oC) will cause a significant drop in brine temperature, mixing will not result to scale deposition since the condensates will acidify the brine pH and inhibit the silica scale deposition in the pipeline (Weres et al., 1981; Hirowatari, 1988). Moreover, the brine will be diluted with non-mineralized condensate fluid minimizing further the tendency to develop silica deposition. In addition, the dissolved components of the brine will buffer the acidity of the dissolve components of the condensate. Mixing of these solutions maybe acceptable however, the risk of SCC increases as the level of chloride is increased and hence corrosion, SCC, and scaling studies of mixed brine and aerated condensate will be the subject of future works.

7.0 CONCLUSIONS

- Field material testing results show that low carbon steel is not resistant to aerated condensate which is saturated with dissolved CO_2 and H_2S gases. Either SUS-304 and SUS-316, is the ideal alloy for long term disposal of the condensate.
- Chemical modeling through stability (Pourbaix) diagram also suggests that this fluid will favor the formation of free Fe^{++} as corrosion products resulting in continuous uniform corrosion along the line.
- The polarization curve of the low carbon steel showed that it is incapable of forming a protective layer. It also suggests a continued breakdown of the protective film.
- The analysis of the corrosion samples exposed to aerated condensate using SEM, EPMA, XRD and X-Ray Fluorescence analyses showed that there are two distinct layers of corrosion along the low carbon steel line. The lower layer is that of pyrite (FeS_2) while the upper layer is that of $FeSO_4.H_2O$. This hydrated ferrous sulfate corrosion is the product formed when H_2S reacts with steel and atmospheric oxygen.

- The polarization experiment showed that SUS-410 (12%Cr martensitic steel) is still susceptible to corrosion. Thus, a more resistant austenitic stainless steel alloyed with Ni and/or Mo is needed for Upper Mahiao condensate reinjection pipeline.

REFERENCES

Borshevska, M. K.A. Lichti and P.T. Wilson (1984). *The Relationship Between Corrosion Products and Corrosion Rates in Geothermal Steam*. Proceedings, The 6th New Zealand Geothermal Workshop. 191 pp.

Forte, N. (1996). *The 125 MW Upper Mahiao Geothermal Power Plant, "The Largest Geothermal steam/binary Combined Cycle Plant Starts-Up"*. Transactions, Vol. 20, pp. 743-748.

Hibara, Y. and M. Tahara (1986). *How to Maintain Geothermal Steam Turbines*. Proceedings, ASME/IEEE Power Generation Conference, Portland, Oregon.

Hirowatari, K. (1988). *Removal and Preventive Methods of Scale Deposition in Geothermal Power Stations*. Chinetsu, Vol. 25, No. 4, pp. 37-38.

Kurata Y., N. Sanada, , H. Nanjo, J. Ikeuchi and K.A. Lichti (1995). *Material Damage in A Volcanic Environment. Proceedings*, World Geothermal Congress, pp. 2409-2413.

Lichti, K.A., C.A. Johnson, P.G.H. McIlhone, P.T. Wilson (1995). *Corrosion of Iron-Nickel Base and Titanium Alloys in Aerated Geothermal Fluids*. Proceedings, World Geothermal Congress, Italy, pp 2375-2380.

Lichti, K.A. S. Soylemezoglu and K.D. Cunliffe (1980). *Geothermal Corrosion and Corrosion Products*. Proceedings, The 2nd New Zealand Geothermal Workshop, pp. 103-108.

Lichti, K.A., S.J. Schwann, S.P. White, N.Sanada, *Y. Kurata, H. Nanjo, J. Ikeuchi and B.W. Christenson (1997). Corrosion in Volcanic Gases*. Proceedings, NEDO International Geothermal Symposium, pp. 154.

Mashall, T. and W.R. Braithwaite (1973). *Corrosion Control in Geothermal Systems*. Unesco, 1973. Geothermal Energy (Earth Sciences, Vol. 12), pp. 151-158.

Mitsubishi Heavy Industries, Ltd. (1989). *Geothermal Power Generation*. Reprinted 1993.

Pound, B.G., M.H. Abdurrahman, M.P. Glucina, R.M. Sharp and G.A. Wright (1979). *The Measurement of Corrosion Rates of carbon Steel in Geothermal Media by the Polarization Resistance Technique*. Proceedings, The 2nd New Zealand Geothermal Workshop, pp. 97-100.

Romanov, V.V. (1969). *Corrosion of Materials: Methods of Investigation*. Translated from Russian (Israel Program for Scientific Translation), pp. 115 - 156.

Salonga, N.D., R.R. Villa, R.G. Arones (1998). *Disposal Management of Steam Condensates from a 125 MW Direct Condensation Power Plant Upper Mahiao, Leyte, Philippines*. Transactions, Vol. 22 pp. 223-227.

Salonga, N.D., R.R. Villa, S.G. Ramos and M.C. Magdadaro (1998). *Pipeline Corrosion in Condensate Solution Containing Carbon Dioxide and Hydrogen Sulfide Upper Mahiao Sector, Leyte, Philippines*. PNOC-EDC Internal Report.

Sanada, N., Y. Kurata, H. Nanjo and J. Ikeuchi (1995). *Material Damage in High Velocity Acidic Fluids*. Transactions, Geothermal Resource Council Vol. 19, pp 359-363.

Uhlig, H.H and R.W. Revie (1985). *Corrosion and Corrosion Control An Introduction to Corrosion Science and Engineering*, 3rd Edition, John Wiley and Sons.

Villa, R.R. and N.D. Salonga (1997). *UMPP STG-20 Turbine Scales and Corrosion Documentation.* PNOC-EDC Internal Report.

Villa, R.R., N.D. Salonga and J.B. Rosell (1997). *Materials Corrosion Testing in Upper Mahiao Steamlines, Leyte, Philippines*. PNOC-EDC Internal Report.

Weres, O., Yee, A. snd Tsao, L. (1981). *Kinetics of Silica Polymerization*, Jnl. Of Colloid and Inter. F. Science.

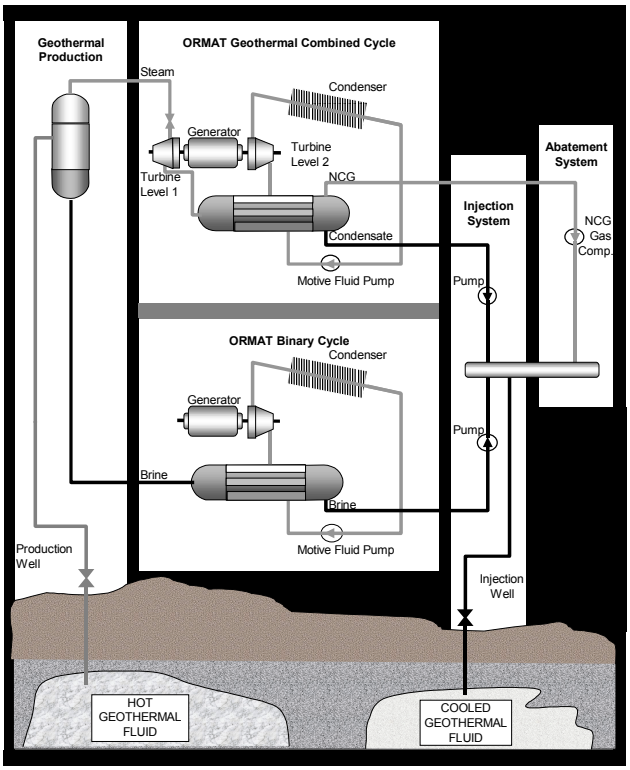

Figure 1: GCCU process flow diagram.

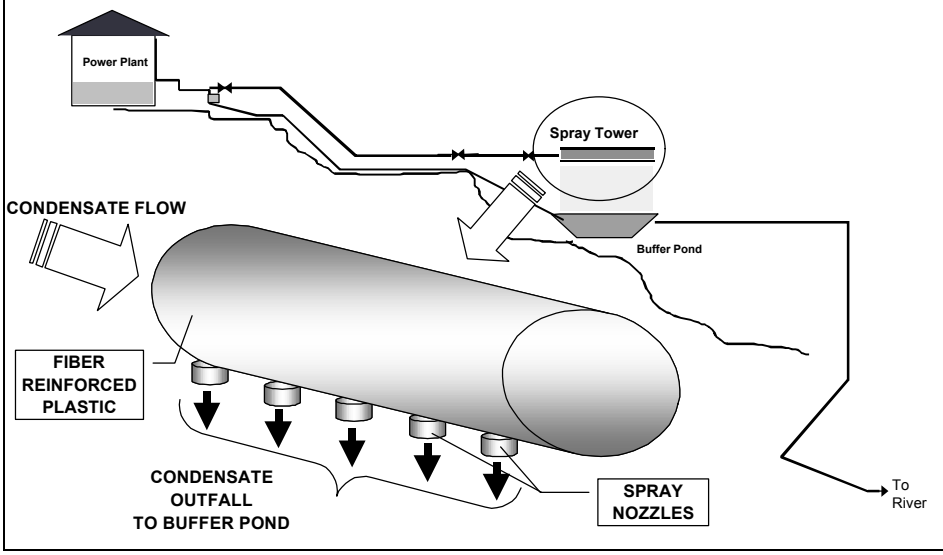

Figure 2: Spray tower as installed prior to river disposal to reduce fluid temperature

Table 1: Ranges of different dissolved chemical constituents of Upper Mahiao condensate. Note that other heavy metal components such as Hg, Cd, Cr and Co co-exist in trace amounts. (D.O. = dissolved oxygen)

Component	Range, ppm	Component	Range, ppm
SiO_2	<0.01-0.26	Cl	3.7-4.4
Na	0.3-3.6	B	3.6-4.4
K	0.1-2.0	HCO_3	16.9-183.0
Fe	0.8-4.0	CO_2	67.2-240.7
As	0.02-0.04	H_2S	2.0-14.5
TDS	4.9-14.3	NH_3	11.9-13.2
pH (H^+ units)	**5.2-5.9**	D.O.	0.04-0.12

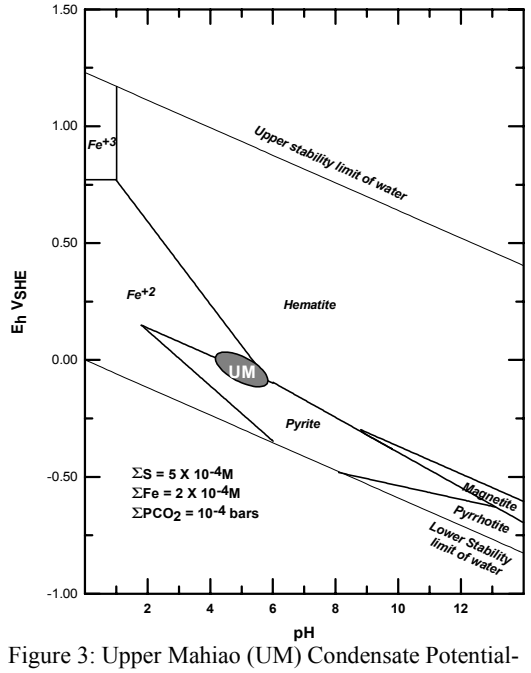

Figure 3: Upper Mahiao (UM) Condensate Potential-pH (Pourbaix) diagram

Table 2: Results of X-Ray Fluorescence and X-Ray Diffraction (XRD) Crystallography (Test 2).

Sample Name		Low Carbon Steel Pipeline Corrosion	
Item Analyzed		X-Ray Fluorescence	
wt % Composition	Fe (as Fe_2O_3)	24.13*	(34.50)**
	Cu (as CuO)	0.05	(0.06)
	Ni (as NiO)	<0.02	( )
	Zn (as ZnO)	0.05	(0.06)
	Al (as Al_2O_3)	0.45	(0.84)
	Si (as SiO_2)	5.59	(11.95)
	Mg (MgO)	<0.02	( )
	Pb (as PbO)	<0.02	( )
	Mn (as MnO_2)	<0.02	( )
	Mo (as MoO_3)	<0.02	( )
	Cr (as Cr_2O_3)	<0.02	( )
	Na (Na_2O)	0.96	(1.30)
	Ca (as CaO)	0.17	(0.23)
	Ti (as TiO_2)	<0.02	( )
	V (V_2O_5)	<0.02	( )
	S (as SO_3)	24.26	(60.57)
	K (as K_2O)	<0.02	( )
	P (as P_2O_5)	0.13	(0.30)
	Sn (as SnO_2)	<0.02	( )
	W (as WO_3)	0.03	(0.04)
	Nb (as Nb_2O_5)	<0.02	( )
	Total		(109.85)
X-Ray Diffraction Crystal Structure Analysis		FeS_2	
		$FeSO_4.H_2O$	
* element value		** oxide value	

Table 3: Composition of metals tested by polarization technique

Material Tested	Chemical composition (wt %)										
	C	Si	Mn	P	S	Ni	Cr	Mo	Cu	N	Others
LCS (IF)	0.002	0.01	0.13	0.004	0.004	-	-	-	-	0.003	-
SUS-410	0.15	1.00	1.00	0.04	0.030	-	11.50 ~ 13.5	-	-	-	-
SUS-304	0.08	1.00	2.00	0.045	0.030	8.00 ~ 10.50	18.00~ 20.0	-	-	-	-
SUS-316	0.08	1.00	2.00	0.045	0.030	10.00 ~ 14.0	16.00 ~ 18.0	2.00 ~ 3.00	-	-	-

Table 4: Chemistry of the Upper Mahiao disposed condensate used as electrolyte during polarization experiment

Sample		**COMPOSITION (mg/kg)**							
	pH	**CO_{2T}**	**HCO_3**	**B**	**Cl**	**SiO_2**	**SO_4**	**NH_3**	**H_2S**
UM-Cond.	5.48	188.1	24.9	4.31	1.83	0.22	<1.0	13.9	21.2
		Na	**K**	**Ca**	**Mg**	**Li**	**Rb**	**Cs**	**Fe**
		0.07	0.54	0.99	1.55	<0.003	<0.003	<0.002	0.58

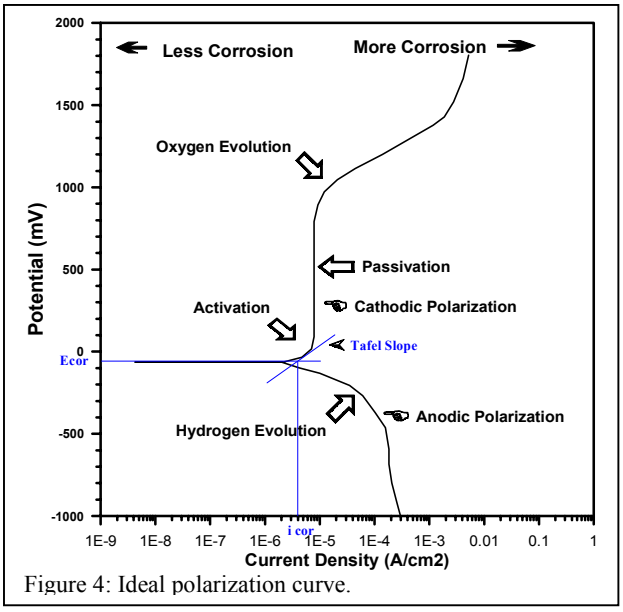

Figure 4: Ideal polarization curve.

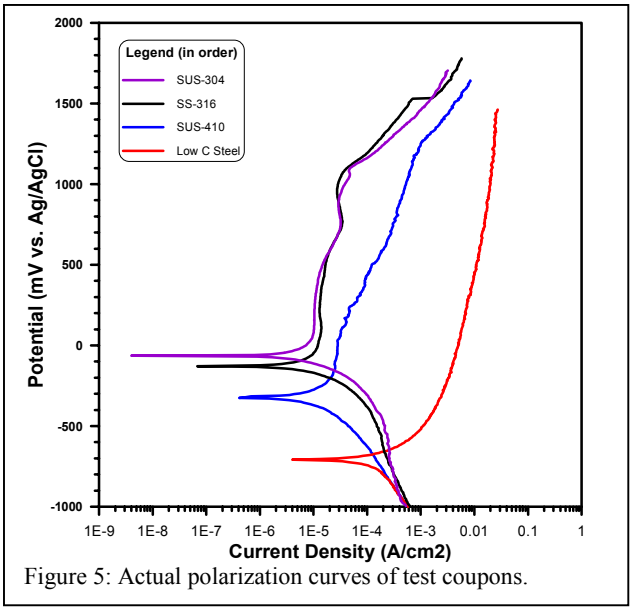

Figure 5: Actual polarization curves of test coupons.

Table 5: Calculated corrosion rates from the polarization experiment at 55°C.

Material Tested	**E_{cor} , mV $V_{Ag/Cl2}$**	**E_{cor} , mV V_{SHE}**	**i_{cor} A/cm_2**	**Corrosion Rate**
SUS-304	-62	+173	4.4 E-7	0.04 mm/yr.
SUS-316	-128	+107	4.4 E-7	0.04 mm/yr.
SUS-410	-325	-90	8.2 E-7	0.075 mm/yr.
Low C Steel (IF)	-710	-475	2.3 E-5	2.10 mm/yr.